p-ISSN 2089 – 0133 e-ISSN 2477-6416
URL : https://jurnal.uns.ac.id/ijap/article/view/74821

DOI : https://doi.org/10.13057/ijap.v13i2.74821

PHOTOCURRENT DENSITY ENHANCEMENT OF DSSC WITH EXISTENCE OF ZnO IN TiO_2 BASED PHOTOANODE

Lusi Safriani*[1], Nurfitriani[1], Ayunita Chintia Celline[1], Annisa Aprilia[1] and Yukio Furukawa[2]

[1]Department of Physics, Faculty Mathematics and Natural Sciences, Universitas Padjadjaran, Bandung, Indonesia
[2]Department of Chemistry and Biochemistry, School of Advanced Science and Engineering, Waseda University. Shinjuku-ku, Tokyo, Japan
* lusi.safriani@phys.unpad.ac.id

Received 11-06-2023, Revised 21-08-2023, Accepted 24-09-2023
Available Online 24-09-2023, Published Regularly October 2023

ABSTRACT

One of the important components of a dye-sensitized solar cell (DSSC) is the photoanode, which plays a critical role in serving as the center of conversion energy. Photoanode consists of a transparent conducting substrate, a semiconductor layer, and dye molecules as sensitizers. Titanium dioxide (TiO_2) is widely used as a photoanode because it is a mesoporous and stable material despite its high recombination rate. TiO_2 is combined with other materials, such as ZnO, to form TiO_2/ZnO composites to reduce the recombination rate and improve electron transport. ZnO is a good choice because it has higher electron mobility than TiO_2 to inhibit recombination. The synthesis process of TiO_2/ZnO composites was carried out using the sol-gel method with variations in the weight percentage of ZnO. The TiO_2/ZnO composite was then applied as a photoanode in DSSC. The J-V measurement results show that the DSSC with TiO_2/ZnO 25wt% composite layer as the photoanode produced the highest efficiency of 0.86%. This increase in efficiency was due to a rise in the photo-current of photoanodes with more ZnO content. The presence of ZnO leads to faster-moving electron transport, reducing recombination and increasing efficiency.

Keywords: DSSC; photoanode; TiO_2; ZnO; composites

Cite this as: Safriani, L., Nurfitriani., Celline, A. C., Aprilia, A., & Furukawa, Y. 2023. Photocurrent Density Enhancement of DSSC With Existence of ZnO in TiO_2 Based Photoanode. *IJAP: Indonesian Joirnal of Applied Physics, 13*(2), 252-261. doi: https://doi.org/10.13057/ijap.v13i2.74821

INTRODUCTION

Dye-sensitized solar cells (DSSC) have attracted much attention as a third-generation photovoltaic technology due to their low cost and easy production process compared to silicone-based solar cells. In 1991, Micheal Grätzel and Brian O'Regan fabricated the first remarkable TiO2-based DSSC, which showed high photo-conversion efficiency (PCE)[1]. The main components of DSSC consist of a photoanode, electrolytes, and counter electrode (CE) [2]. Photoanode plays an important role where absorbed light is converted into electricity. The material used as a photoanode is a thin layer of semiconductor oxide, such as TiO_2 [3], ZnO [4], and SnO_2 [5], which is deposited on a transparent conducting substrate. The photoanode layer is also where the dye is located to extend the range of the absorption spectrum to visible light. Other components, the electrolyte and counter electrode, are necessary for the charge regeneration of dye and for collecting electrons from the external circuit, respectively [6]. The enhancement of DSSC's performance has been reported by the use of multi-structured metal

oxide semiconductors for the effective electron transport and higher surface areas for the absorption of dyes [7] as well as metal oxides nanocomposites for the efficient charge separation [8] and reducing recombination process [9].

Among various metal oxide semiconductors, titanium dioxide (TiO_2) has been widely used as a photoanode in DSSC due to its excellent structural, electrical, optical, and chemical properties [7-10]. TiO_2 has three polymorphs, i.e., anatase and brookite, which are metastable, while rutile is the most stable polymorph [11]. Despite the advantages of TiO_2, its photoanode-based DSSC efficiency is still inferior to other solar cells. This is due to TiO_2's limitations of efficient charge transfer, leading to multiple recombination processes and reduced DSSC efficiency [12 -14]. To address this issue, researchers combine TiO_2 with other materials with high electron transport rates to decrease recombination, thereby increasing DSSC efficiency. One example of such a material is zinc oxide (ZnO), which has high electron mobility [15] and a bandgap similar to TiO_2 [16]. ZnO is also easy to synthesize in nanoparticle production, making it a suitable material for combining with TiO_2 [17-18].

Various methods have been used to obtain TiO_2-ZnO nanocomposites on different nanostructures to improve DSSC performance. Boro et al. have used TiO_2-ZnO with other nanostructures whose efficiency ranges from 0.51-9% [19]. Thate et al. fabricated DSSC-based TiO_2-ZnO nanocomposites photoanode with a 3:1 ratio through chemical bath deposition, which shows an efficiency of 0.74% [20]. The solution combustion approach was utilized by Deepa et al. to produce TiO_2-ZnO nanocomposites, which resulted in a low power efficiency conversion of 0.00175% [21]. This study combined ZnO with TiO2 with different amounts of ZnO using the sol-gel method to produce TiO_2/ZnO composites, which were then used as photoanodes in DSSCs. The chemical composition of TiO_2 and ZnO in the composites was examined using x-ray fluorescence (XRF), while their crystal structure and optical properties were characterized using x-ray diffraction (XRD) UV-Vis spectrophotometer. The performance of DSSCs with TiO_2/ZnO composites as photoanodes was studied from the J-V curve data.

METHOD

Materials used in preparing TiO_2 and TiO_2-ZnO composite were titanium (IV) n-butoxide (97%, Sigma-Aldrich), nitric acid (65%, Merck), acetic acid (100%, Merck), zinc acetate dihydrate (Merck), triton-X (Sigma Aldrich) and ethanol as solvent. Mosalyte TDE-250 (Solaronix), ruthenizer 535-bis TPA (Solaronix), and chenodeoxycholic acid (Solaronix) were used to fabricate DSSC. All chemicals were used as received and without further purification.

The synthesis of TiO_2-ZnO was started by dissolving 0.1 M titanium (IV) n-butoxide in 10 ml of ethanol and then stirring at 65°C. Before use, 0.05 M nitric acid was diluted in deionized water. The nitric acid solution was added dropwise, then the appropriate amount of 0.1 M zinc acetate dihydrate (13 wt% and 25 wt%) was added and further stirred for three hours to obtain a white solution. After being kept for 24 hours, the precipitate was annealed at 400°C for 2 hours. A paste of TiO_2-ZnO composite was prepared by adding acetic acid and triton-X to TiO_2-ZnO powder.

The photoanode layer was obtained by depositing a paste of the TiO_2-ZnO composite on the FTO substrate using the doctor blade technique. The layer was annealed at 450°C for 15 minutes to produce a crystalline structure of TiO_2 and ZnO. Prior to use, ruthenium 535-TBA and chenodeoxycholic were dissolved in ethanol. Photoanode TiO_2-ZnO was immersed in the above

solution overnight. The photoanode was stacked with the counter electrode using suryln, and finally, the mosalyte as electrolyte was injected through a hole in the counter electrode.

RESULTS AND DISCUSSION

Figure 1 exhibits the XRD patterns of a thin TiO_2 and TiO_2/ZnO composite layer. The XRD patterns follow the Crystallography Open Database (COD) data standard no. 00-901-5662 for rutile phase of TiO_2, no. 00-901-5292 for anatase phase of TiO_2, and no. 00-901-1662 for zincite of ZnO. The diffraction pattern of TiO_2 shows dominant diffraction peaks at (110), (101), (200), and (211), which confirms that it has a rutile phase along with a few minor peaks of anatase. The diffraction pattern of the TiO_2/ZnO composite consists of a dominant rutile phase, a minor anatase phase, and several peaks indicating ZnO peaks that overlap with the peaks of the rutile phase. In the TiO_2/ZnO composite sample, it was seen that with the addition of ZnO to TiO_2, the diffraction peak shifted to a larger value of 2θ. The crystallinity of the TiO_2/ZnO composite decreased with increasing ZnO content. A similar result has been observed by Rajkumar et al. [22]. The XRD results confirmed the successful synthesis of a composite consisting of anatase TiO_2 and zincite ZnO. The lattice parameters of TiO_2 rutile, TiO_2 anatase, and ZnO zincite that have been calculated are presented in Table 1. We found that both TiO_2 rutile and anatase have tetragonal structures, while ZnO wurtzite has a hexagonal structure.

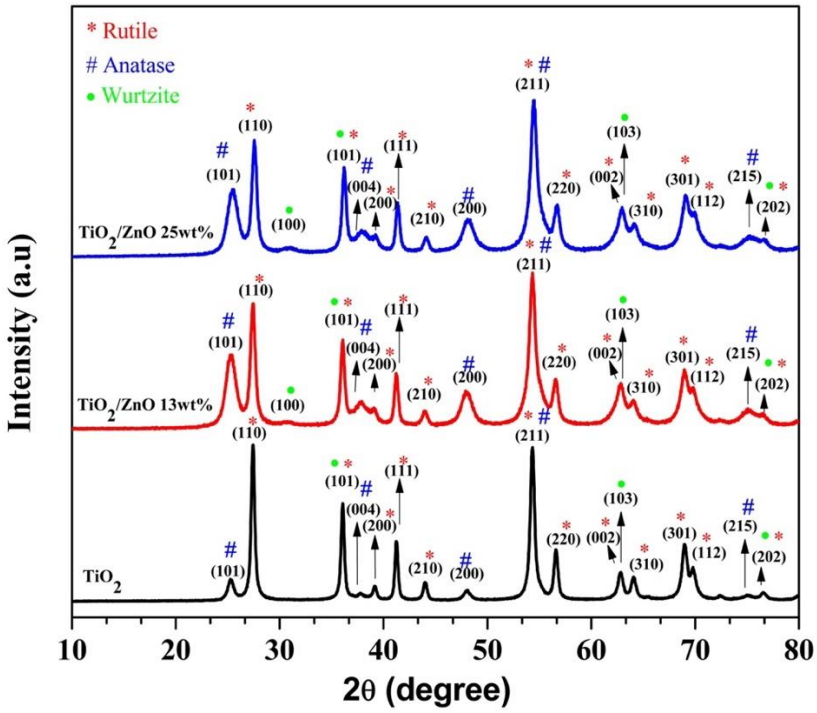

Figure 1. Diffraction patterns of TiO_2 and TiO_2/ZnO composite at 13 wt% and 25 wt% of ZnO content.

The average crystallite size of TiO_2 and TiO_2-ZnO with ZnO content 13 wt% and 25 wt% were calculated using Debye Scherrer's equation based on the full width at half maximum (FWHM) of Bragg peaks from the diffraction patterns shown in Equation 1. In Equation 1, k is the Scherrer constant (0.9), λ is the wavelength of the X-ray irradiation (0.15 nm), β is the full width at half maximum (FWHM), and θ is the X-ray diffraction peak. Table 2 shows crystallite size TiO_2 rutile, TiO_2 anatase, and ZnO wurtzite in samples of TiO_2, TiO_2/ZnO 13 wt%, and TiO_2/ZnO 25 wt%. It was found that both crystallite size of rutile and anatase decreased with

an increase in ZnO content. The presence of ZnO may inhibit the growth of both rutile TiO_2 and anatase TiO_2.

Table 1. Lattice parameters and crystal structure of TiO_2 rutile, TiO_2 anatase, and ZnO wurtzite.

Crystal phase	Lattice parameters		Crystal structure
	a (Å)	c (Å)	
Rutile TiO_2	4.59	2.96	Tetragonal
Anatase TiO_2	3.78	9.51	Tetragonal
Wurtzite ZnO	3.25	5.21	Hexagonal

Table 2. Crystallite size TiO_2 rutile, TiO_2 anatase and ZnO wurtzite in sample of TiO_2, TiO_2/ZnO 13 wt% and TiO_2/ZnO 25 wt%.

Sample	Crystallite size (nm)		
	Rutile	Anatase	Wurtzite
TiO_2	19.81	16.00	-
TiO_2-ZnO 13 wt%	14.69	7.85	18.14
TiO_2-ZnO 25 wt%	14.69	8.01	18.53

$$D = \frac{k\lambda}{\beta \cos\theta} \quad (1)$$

The TiO_2-ZnO composite was examined using XRF to confirm the presence of ZnO and its chemical composition. Table 3 displays the amount of TiO_2 and ZnO present in each sample. When the quantity of ZnO precursor was increased, the mass percentage of ZnO in the TiO_2-ZnO composite was doubled. The XRF results validated the presence of ZnO in the TiO_2/ZnO composite, which corresponded with the XRD measurements.

Table 3. Chemical composition of TiO_2 and TiO_2/ZnO composite.

Sample	TiO_2 content (wt%)	ZnO content (wt%)
TiO_2	99.98	-
TiO_2-ZnO 13wt%	92.87	7.21
TiO_2-ZnO 25 wt%	84.93	15.05

Figure 2 presents the UV-Vis absorption spectra of TiO_2 and TiO_2-ZnO composite. The maximum absorption at a wavelength of around 300 nm of TiO_2 was higher than that of TiO_2/ZnO composite, possibly due to the presence of ZnO. The absorption edge also varied across all samples. Using the Tauc plot method depicted in Figure 3 [23], we calculated the energy band gap of TiO_2, TiO_2-ZnO 13 wt%, and TiO_2-ZnO 25 wt% to be 3.07 eV, 2.84 eV, and 2.81 eV, respectively. In the TiO_2/ZnO composites, the bandgap decreased due to the expansion of the conduction and valance bands of TiO_2, which was attributed to the variation of ZnO content in TiO_2. This modification led to a shift in band gap from 3.07 eV (pure TiO_2) to 2.81 eV (TiO_2-ZnO 25 wt%). The presence of ZnO has therefore modified the electronic structure of TiO_2.

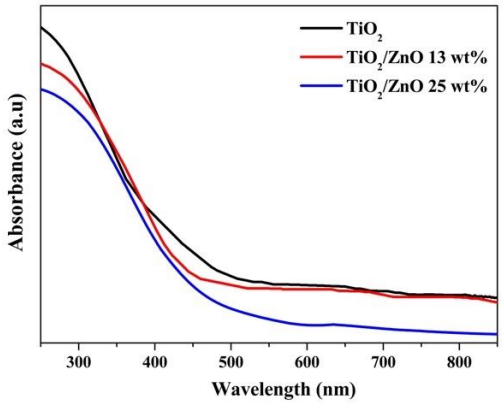

Figure 2. UV-Vis Spectra of TiO_2 and TiO_2/ZnO composite at 13 wt% and 25 wt% of ZnO content.

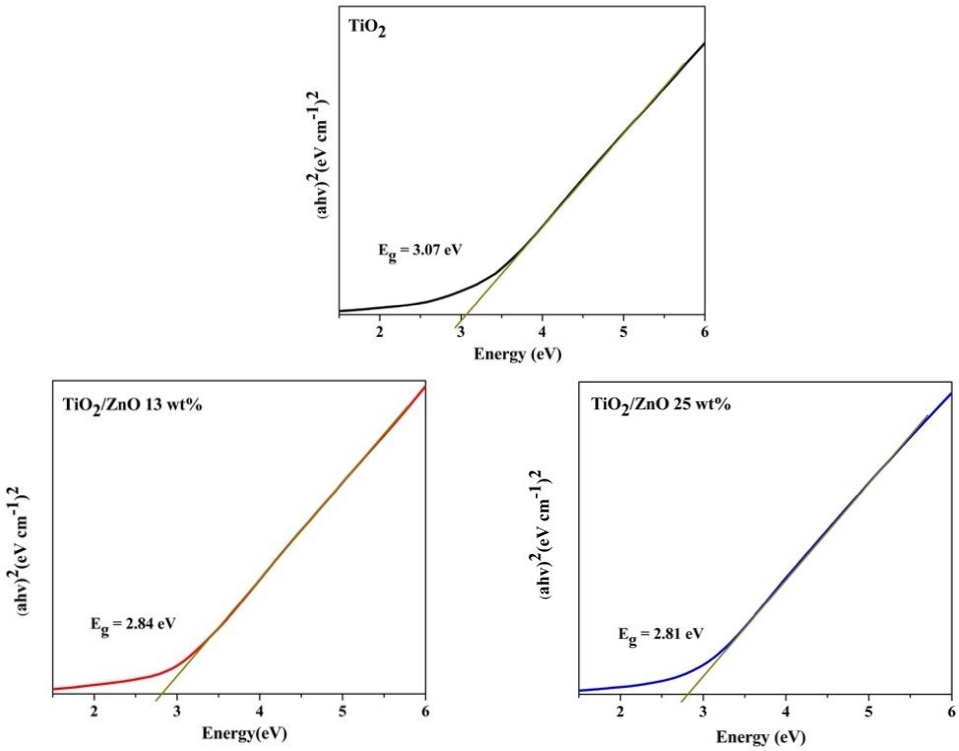

Figure 3. The bandgap of TiO_2 and TiO_2/ZnO composite was calculated using Tauc plots.

In Figure 4, we can observe the SEM image of TiO_2 and TiO_2/ZnO composites that were obtained through the doctor blade technique at different concentrations. Figure 4(a) shows spherical structures with agglomerated TiO_2 particles, which do not appear to have many pores. On the other hand, Figures 4(b) and 4(c) clearly show the porous structure resulting from the addition of ZnO. However, with the addition of 25wt% ZnO to TiO_2, the agglomeration of TiO_2 occurred. For optimal performance in a DSSC, the TiO_2 and TiO_2-ZnO composite photoanodes should have a porous structure to increase dye loading.

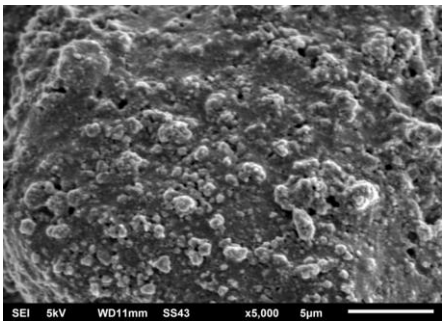

(a)

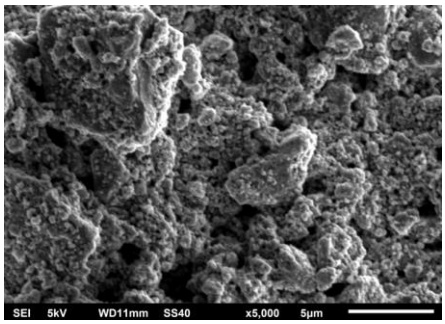

(b)

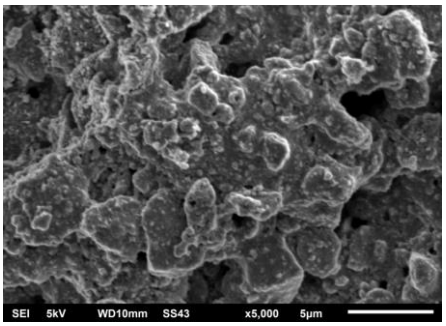

(c)

Figure 4. Top-view SEM images of (a) TiO_2 (b) TiO_2/ZnO 13wt% and (c) TiO_2/ZnO 25wt%

The performance of DSSC was evaluated through a J-V measurement, which determined the short circuit photocurrent density (J_{SC}) and open circuit photovoltage (V_{OC}) of the TiO_2 and TiO_2-ZnO composite photoanodes. Figure 5 displays the $J - V$ curve, with an irradiation source of white light from an Xe lamp at an intensity of 100 mW/cm2. The filling factor (FF) and efficiency (η) of DSSC were calculated using Equations 2 and 3, respectively, and all resulting data has been summarized in Table 4.

$$FF = \frac{V_M J_M}{V_{OC} J_{SC}} \tag{2}$$

with V_M is the maximum photovoltage and J_M is the maximum photocurrent density.

$$\eta = \frac{V_{OC} J_{SC} FF}{P_{in}} \tag{3}$$

where P_{in} is the power of light irradiation.

The TiO_2 photoanode produced a $\mathbf{J_{SC}}$ of 0.55 mA/cm2, $\mathbf{V_{OC}}$ of 0.57 V, and FF of 38.58%, resulting in an efficiency of only 0.12%. However, when ZnO was added to the TiO_2 photoanode, the $\mathbf{J_{SC}}$ increased significantly, reaching 2.07 mA/cm^2 and 2.30 mA/cm^2 with the addition of 13 wt% and 25 wt% ZnO, respectively. Furthermore, the addition of ZnO increased the $\mathbf{V_{OC}}$ from 0.57 V to 0.70 V at both 13 wt% and 25 wt% concentrations. The improvement in both $\mathbf{J_{SC}}$ and $\mathbf{V_{OC}}$ was due to the higher electron mobility of ZnO compared to TiO_2, leading to increased electron transport to the FTO electrode and reduced electron-hole recombination in DSSC. The increase in $\mathbf{J_{SC}}$ was also observed in the UV-Vis spectrum, where the energy band gap decreased as the amount of ZnO increased, modifying the electronic structure of TiO_2. The FF also increased with the addition of ZnO, mainly due to the enhancement of $\mathbf{J_{SC}}$. The DSSC

efficiency of the TiO_2/ZnO 13wt% and TiO_2/ZnO 25wt% photoanodes were 0.69% and 0.86%, respectively.

To analyze the series resistance of a DSSC, we can use an equivalent circuit depicted in Figure 6. This circuit models a solar cell with a diode acting as a photocurrent source, along with a shunt resistance ($\mathbf{R_{sh}}$) and series resistance ($\mathbf{R_s}$) [2]. We can calculate $\mathbf{R_{sh}}$ and $\mathbf{R_s}$ using Equation 4 [6]. The ideality factor (n) represents the recombination process within the cell, while $\mathbf{J_{ph}}$ is the photogenerated current density and $\mathbf{J_0}$ is the dark saturation current density and $\mathbf{V_t}$ is voltage of Boltzmann factor at 298 K ($\mathbf{V_t = (k_B\,T)/q \cong 25.85\ mV}$).

$$\mathbf{J = \frac{R_{sh}}{R_{sh}+R_s}\left\{J_0\left[\exp\left(\frac{q(V-JR_s)}{m\,k_B T}\right)-1\right]+\frac{V}{R_{sh}}\right\}-J_{ph}} \qquad (4)$$

In Table 4, the DSSC parameters based on the J-V curve and fitting using Eq. 4 are presented. By analyzing the parameters of $\mathbf{R_{sh}}$ and $\mathbf{R_s}$ from the fitting curve, we can assess the quality of the DSSC. $\mathbf{R_{sh}}$ and $\mathbf{R_s}$ play a significant role in the DSSC's performance. $\mathbf{R_{sh}}$ is caused by crystal defects at the interface between the dye and semiconductor layer of the photoanode, leading to leakage. $\mathbf{R_s}$ is the resistance between the cells of the TiO_2 layer on transport electron. Ideally, $\mathbf{R_s}$ should be zero while $\mathbf{R_{sh}}$ should be infinite. The smaller the $\mathbf{R_s}$ value and the larger the $\mathbf{R_{sh}}$ value, the better the DSSC parameters. This study discovered that $\mathbf{R_{sh}}$ had a consistent order of 10^3 across all samples, which is not sufficient to generate a high photocurrent. We suspect that the TiO_2 and TiO_2/ZnO layers contain many defects that trap electron transport. Furthermore, among the three samples, TiO_2/ZnO 25 wt% as the photoanode layer had the lowest value of Rs, resulting in the highest efficiency value. We believe that the addition of ZnO, which has high electron mobility, contributed to the increase in photocurrent.

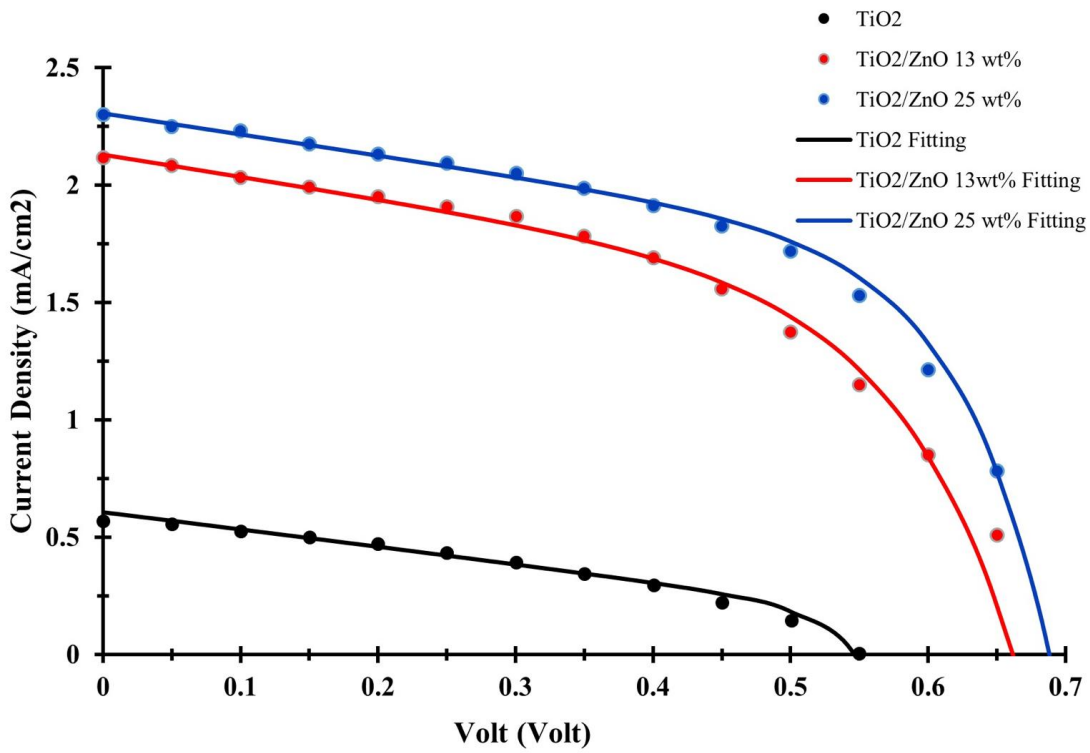

Figure 5. Photocurrent density and voltage of TiO_2 and TiO_2/ZnO based photoanode

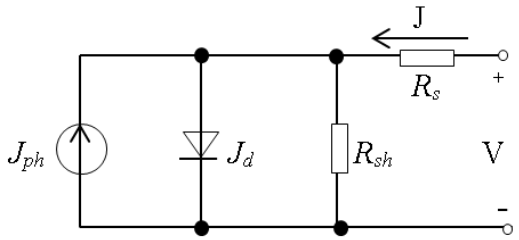

Figure 6 Equivalent circuit of a single diode solar cell [2]

The ideal factor m in Equation 4 indicates the quality of the device. The value of m depends on the photocurrent, voltage, temperature, and junction between layers in the DSSC. We found that in the TiO_2/ZnO layer, the m value exceeds 2, which indicates that the connection formed is not good enough [24]. It is likely that ZnO forms defects on the TiO_2 surface and acts as recombination centers at the interface of TiO_2/ZnO/dye/electrolyte [25]. However, compared to the TiO_2 photoanode, the presence of ZnO increases electron mobilization, resulting in faster electron transport, reduced recombination, and improved DSSC efficiency [19]

Table 4. Parameters of DSSC based on J-V curve and fitting using Eq. 4.

Photoanode	J_{SC} (mA/cm^2)	V_{OC} (Volt)	FF (%)	η (%)	R_s (Ω)	R_{sh} (Ω)	m
TiO_2	0.57	0.55	38.58	0.12	$5.0x10^2$	$7.9x10^3$	1.5
TiO_2/ZnO 13 wt%	2.07	0.70	47.33	0.69	$5.0x10^1$	$9.0x10^3$	3.4
TiO_2/ZnO 25 wt%	2.30	0.70	53.38	0.86	$1.5x10^1$	$7.0x10^3$	2.6

CONCLUSION

The TiO_2/ZnO composite has been successfully synthesized using the sol-gel method. XRF measurements indicated the presence of ZnO compounds in the TiO_2/ZnO samples, with weight percentages of 7.21% and 15.05% respectively. The addition of ZnO to the TiO_2/ZnO composite was found to decrease the energy gap to 2.8 eV, as shown by UV-Vis spectra. SEM images revealed the presence of pores with the addition of ZnO. The use of TiO_2/ZnO composite with a greater weight percentage of ZnO resulted in the highest efficiency of 0.86%, attributable to the highest photocurrent of 2.30 mA/cm^2. These results indicate that adding ZnO contributes to an increase in photocurrent and efficiency, by facilitating faster electron transport and reducing the recombination process.

ACKNOWLEDGMENTS

The authors would like to acknowledge to Universitas Padjadjaran for financial supporting under the project of Hibah Riset Unpad contract no.1549/UN6.3.1/PT. 00/2023.

REFERENCES

1. O'Regan, B. and Grätzel, M. 1991. A low cost, high-efficiency solar cell based on dye-sensitized colloidal TiO2 films. Nature, 353, 737-740, DOI: 10.1038/353737a0.

2. Sharma, K., Sharma, V., & Sharma, S. S. 2018. Dye-Sensitized Solar Cells: Fundamentals and Current Status. Nanoscale Res. Lett., 13(381), 1-46, DOI: 10.1186/s11671-018-2760-6.

3. González-Verjan, V. A., Trujillo-Navarrete, B., Félix-Navarro, R. M., de León, J. N. D., Romo-Herrera, J. M., Calva-Yáñez, J. C., Hernández-Lizalde, J. M., and Reynoso-Soto, E. A. 2020. Effect of TiO2 particle and pore size on DSSC efficiency. Materials for Renewable and Sustainable Energy, 9(13), 1-8, DOI: 10.1007/s40243-020-00173-7.

4. Gan, Y. K., Zakaria, N. F., Mohamad, I. S., and Norizan, M. N. 2020. The effect of ZnO photoanode solution ageing to the performance of dye-sensitized solar cell (DSSC). AIP Conf. Proc., 2203, 020048, DOI: 10.1063/1.5142140.

5. Dimarco, B. N., Sampaio, R. N., James, E. M., Barr, T. J., Bennett, M. T., and Meyer, G. J. 2020. Efficiency Considerations for SnO2-Based Dye-Sensitized Solar Cells. ACS Appl. Mater. Interfaces, 12(21), 23923–23930, DOI: 10.1021/acsami.0c04117.

6. Gong, J., Sumathy, K., Qiao, Q., and Zhou, Z. 2017. Review on dye-sensitized solar cells (DSSCs): Advanced techniques and research trends. Renewable Sustainable Energy Rev., 68, 234–246, DOI: 10.1016/j.rser.2016.09.097.

7. Pan, M., Huang, N., Zhao, X., Fu, J., and Zhong, X. 2013. Enhanced efficiency of dye-sensitized solar cell by high surface area anatase-TiO2-modified P25 paste. J. Nanomater., 2013, 760685, DOI: 10.1155/2013/760685.

8. Ge, F., Xu, F., Gong, K., Liu, D., Li, W., Wang, L., and Zhou, X. 2022. Sensitizers designed toward efficient intramolecular charge separation for p-type dye-sensitized solar cells. Dyes and Pigments, 200, 110127, DOI: 10.1016/J.DYEPIG.2022.110127.

9. Nur Azella Zaine, S., Muti Mohamed, N., Khatani, M., Eskandar Samsudin, A., and Umair Shahid, M. 2020. Trap State and Charge Recombination in Nanocrystalline Passivized Conductive and Photoelectrode Interface of Dye-Sensitized Solar Cell. Coatings, 2020, 10(3), 284, DOI: 10.3390/coatings10030284.

10. Supriyanto, A., Saputri, D. G., Ahmad, M. K. Bin, Sutomo, A. D., and Ramelan, A. H. 2023. Influence of Coating a TiO2 Electrode with DN-F05 and DN-F05-Ag on the Photovoltaic Performance of DSSC Solar Cells. Appl. Sci., 13(13), 7459. DOI: 10.3390/app13137459.

11. Castrejón-Sánchez, V. H., López, R., Ramón-González, M., Enríquez-Pérez, Á., Camacho-López, M., and Villa-Sánchez, G. 2019. Annealing control on the anatase/rutile ratio of nanostructured titanium dioxide obtained by sol-gel. Crystals, 9(22), 1-12, DOI: 10.3390/cryst9010022.

12. Grätzel, M. 2001. Photoelectrochemical cells. Nature, 414, 338, DOI: 10.1038/35104607.

13. Mahalingam, S., and Abdullah, H. 2016. Electron transport study of indium oxide as photoanode in DSSCs: A review. Renewable Sustainable Energy Rev., 63, 245–255, DOI: 10.1016/j.rser.2016.05.067, DOI: 10.1016/j.rser.2016.05.067.

14. Yao, N., Huang, J., Fu, K., Deng, X., Ding, M., Zhang, S., Xu, X., and Li, L. 2016. Reduced interfacial recombination in dye-sensitized solar cells assisted with NiO:Eu3+,Tb3+ coated TiO2 film. Sci. Rep., 6, 31123, DOI: 10.1038/srep31123.

15. Ramya, M., Nideep, T. K., Nampoori, V. P. N., and Kailasnath, M. 2021. The impact of ZnO nanoparticle size on the performance of photoanodes in DSSC and QDSSC: a comparative study. J Mater Sci: Mater Electron, 32, 3167–3179, DOI: 10.1007/s10854-020-05065-0.

16. Kamarulzaman, N., Kasim, M.F., and Rusdi, R. Band Gap Narrowing and Widening of ZnO Nanostructures and Doped Materials. 2015. Nanoscale Res. Lett., 10, 346. DOI: 10.1186/s11671-015-1034-9.

17. Agrawal, A., Siddiqui, S. A., Soni, A., Sharma, G. D., and Shrivastava, D. R. 2020. ZnO nanoparticles based dye sensitized solar cell: Fabrication and characterization. AIP Conf. Proc., 2294, 030005, DOI: 10.1063/5.0031753.

18. Ramya, M., Nideep, T. K., Nampoori, V. P. N., and Kailasnath, M. 2021. Solvent assisted evolution and growth mechanism of zero to three dimensional ZnO nanostructures for dye sensitized solar cell applications. Sci. Rep., 11, 6159 DOI: 10.1038/s41598-021-85701-9.

19. Boro, B., Gogoi, B., Rajbongshi, B. M., and Ramchiary, A. 2018. Nano-structured TiO2/ZnO nanocomposite for dye-sensitized solar cells application: A review. Renewable Sustainable Energy Rev., 81, 2264–2270, DOI: 10.1016/j.rser.2017.06.035.

20. Thate, A.G., Pakhare, K.S., Patil, S.S., and Bhuse, V.M. 2023. Fabrication of TiO2-ZnO nanocomposite photoanodes to enhance the dye-sensitized solar cell efficiency. Res. Chem. Intermed., 49, 147–168 (2023). DOI: 10.1007/s11164-022-04878-4.

21. Deepa, H. A., Madhu, G. M., and Venkatesham, V. 2019. Performance evaluation of DSSC's fabricated employing TiO2 and TiO2-ZnO nanocomposite as the photoanodes. Mater. Today: Proc., 46, 4579–4586. DOI: 10.1016/j.matpr.2020.09.711.

22. Rajkumar, N., Kanmani, S. S., and Ramachandran, K. 2011. Performance of dye-sensitized solar cell based on TiO2:ZnO nanocomposites. Adv. Sci. Lett., 4(2), 627–633. DOI: 10.1166/asl.2011.1265

23. Makuła, P., Pacia, M., and Macyk, W. 2018. How To Correctly Determine the Band Gap Energy of Modified Semiconductor Photocatalysts Based on UV-Vis Spectra. J. Phys. Chem. Lett., 9 (23) 6814–6817. DOI: 10.1021/acs.jpclett.8b02892.

24. Hadke, S., Huang, M., Chen, C., Tay, Y. F., Chen, S., Tang, J., and Wong, L. 2022. Emerging Chalcogenide Thin Films for Solar Energy Harvesting Devices. Chem. Rev., 122 (11), 10170–10265). DOI: 10.1021/acs.chemrev.1c00301.

25. Rani, M., and Tripathi, S. K. 2016. Electron transfer properties of organic dye sensitized ZnO and ZnO/TiO2 photoanode for dye sensitized solar cells. Renewable Sustainable Energy Rev., 61, 97–107, DOI: 10.1016/j.rser.2016.03.012.